Available online at www.sciencedirect.com
SCIENCE DIRECT®
Planetary and Space Science 52 (2004) 397–414
Planetary and Space Science
www.elsevier.com/locate/pss

On the water abundance in the atmosphere of Jupiter

M. Roos-Serote[a,*], S.K. Atreya[b], M.K. Wong[c], P. Drossart[d]

[a] *Lisbon Astronomical Observatory, Tapada da Ajuda, 1349-018 Lisbon, Portugal*
[b] *Department of Atmospheric, Oceanic and Space Sciences, University of Michigan, Ann Arbor, MI 48109-2143, USA*
[c] *NASA/Goddard Space Flight Center, USA*
[d] *Observatory of Paris at Meudon, 5 Place J. Janssen, 92195 Meudon Cedex, France*

Received 20 January 2003; accepted 16 June 2003

Abstract

In this paper, we attempt to place constraints on the possible global abundance of water and the average vertical cloud structure in the atmosphere of Jupiter. Based on the analysis of the Galileo Near-Infrared Mapping Spectrometer data, we find that in the atmosphere of Jupiter down to 6–8 bar, particularly in the North Equatorial Belt (NEB) region, the overall O/H ratio is *compatible* with one or more times the solar value of this ratio. We also find that if water clouds form at the levels where they are expected from thermochemical equilibrium calculations for a given deep O/H ratio, then subsolar values of the O/H ratio cannot be reconciled with the analyzed data. However, these results are dependent on the model atmosphere, in particular the detailed vertical distribution of cloud opacity. Therefore, they should be considered with care, until new observations on the vertical cloud structure become available. The water vapor mixing ratio in the NEB displays large spatial variations. The same set of data yield subsaturated mixing ratios of ammonia to atmospheric levels of about 4 bar. This depletion of ammonia to great depths, as seen by the Galileo Probe in the hot spot where it entered, appears to be a common phenomenon in the entire NEB.

Keywords: Jupiter; Atmosphere; Composition; Structure; Infrared data

1. Introduction

A knowledge of the composition of the planets and their atmospheres is a key element for our understanding of the formation and evolution of the Solar System. The atmosphere of Jupiter has been slowly revealing its secrets over the past four decades. In particular, the analysis of in situ measurements by the Galileo Probe, combined with space- and earth-based remote sensing, has resulted in an important leap forward in our understanding of this planet. We have learned that Jupiter is a complex object, with strong global and local dynamics, and enriched in heavy elements relative to the Sun. It is found that on Jupiter C/H, N/H, S/H, Ar/H, Xe/H and Kr/H are all enhanced relative to their solar values by a factor 3 ± 1 (Atreya et al., 2003). Yet, the debate concerning the O/H ratio has still not been settled satisfactory. This is due to the fact that water vapor, the main reservoir of oxygen (except for a tiny amount of CO), could not be measured in situ in the deep well-mixed atmosphere of Jupiter. The Galileo Probe went into the so-called 5-μm hot spot, a dry region in Jupiter's atmosphere. The data showed that the water vapor mixing ratio increased 10 fold between 12 and 19 bar and showed a trend of continuous increase with depth. No data were retrieved from below this region. This observation corresponds to a maximum $(O/H)_{Jupiter}$ of $0.35 \times (O/H)_{Sun}$ (Niemann et al., 1998; Atreya et al., 2003). However, as water is expected to be the original carrier of heavy elements to Jupiter, oxygen is predicted to be enriched by at least as much as the other heavy elements according to the icy planetesimals model (Owen et al., 1999; Atreya et al., 2003), or by at least 9.4 times the solar O/H value according to the clathrate hydrate model (Gautier et al., 2001a, b). So, the knowledge of the global O/H ratio is critical to the models of formation of Jupiter and its atmosphere.

Tropospheric water vapor can be measured spectroscopically in the 4.5–5-μm region of the Jovian spectrum and many past studies have been dedicated to this measurement using different instruments. In particular, attempts to measure Jupiter's atmospheric water vapor abundance by remote sensing from Voyager observations (Hanel et al., 1979;

* Corresponding author. Tel.: +351-21-36-15-746; fax: +351-21-36-16-752.
E-mail address: roos@oal.ul.pt (M. Roos-Serote).

0032-0633/$ - see front matter © 2003 Elsevier Ltd. All rights reserved.
doi:10.1016/j.pss.2003.06.007

Kunde et al., 1982; Drossart and Encrenaz, 1982; Bjoraker et al., 1986; Carlson et al., 1992) and from Galileo orbiter data (Irwin et al., 1998, 2001; Nixon et al., 2001; Roos-Serote et al., 1998, 1999, 2000) have been made. Cassini observations of Jupiter are presently being analyzed. The Infrared Space Observatory (ISO) obtained some very good data, but at very low spatial resolution (Encrenaz et al., 1996). Ground-based observations have been difficult due to overlapping terrestrial water lines. However, the pressure broadening of lines in the Jovian 5-μm window is larger than that in the Earth's atmosphere. Recent improvements in the resolving power of ground-based observations now allow more accurate ground-based measurements (Bjoraker et al., 2002).

Most of the spectroscopic observations focus on the North Equatorial Belt (NEB) and the hot spots within it. The NEB is a region where the higher-lying clouds are less opaque allowing radiation to escape from the troposphere more easily. Deep tropospheric levels (down to about 8 bar) can be sounded in the 5-μm window. Hot spots are regions, mostly within the NEB, that have almost no high clouds, and are thus very bright in the 5-μm window (Ortiz et al., 1998). They are thought to be related to wave phenomena in the atmosphere (Friedson and Orton, 1999; Showman and Dowling, 2000; Baines et al., 2002). Interpretations of Voyager Infrared Radiometer and Interferometer Spectrometer (IRIS) NEB and hot spot spectra at 5 μm by different teams have led to quite different conclusions concerning the deep atmospheric O/H ratio and the vertical cloud structure (Kunde et al., 1982; Drossart and Encrenaz, 1982; Bjoraker et al., 1986; Carlson et al., 1992). Estimates of $(O/H)_{Jupiter}$ range from much less than solar to several times solar, and the models always included water clouds at different levels in the atmosphere (4–7 bar). Analysis of Galileo 5-μm Near-Infrared Mapping Spectrometer (NIMS) hot spot data by different groups (Nixon et al., 2001; Irwin et al., 1998, 2001; Roos-Serote et al., 1998, 1999, 2000) show a more coherent picture. This picture also corroborates the scenario measured by the Galileo Probe, i.e. an extremely dry atmosphere (in water vapor) with hardly any clouds. In fact, no significant clouds were detected by the Galileo Probe at pressures greater than 1.6 bar (Ragent et al., 1998). The reanalysis of the Voyager IRIS data by Roos-Serote et al. (1999) suggest that a calibration problem for wavelengths less than 5 μm could be the reason for the fact that deep water clouds were always needed to fit the Voyager data, even for hot spot spectra.

From thermodynamical modeling of the Jovian atmosphere it has been possible to predict the possible cloud structure (Weidenschilling and Lewis, 1973; Atreya and Romani, 1985; Atreya et al., 1999). It is found that in the case of a three-fold enhancement of the condensibles (NH_3, H_2S, and H_2O) relative to the solar elemental ratios (N/H, S/H, O/H), three cloud layers are expected: a water cloud with a base at approximately 7 bar, an ammonium hydrosulfide (NH_4SH) cloud with a base at 2.61 bar, and an ammonia ice cloud with a base at 0.84 bar (Atreya et al., 1999). Atreya et al. (1999) simulated the cloud structure as found by the Galileo Probe in a hot spot region. They find that for a water cloud to form at 1.6 bar, the deepest level where the Galileo Probe detected any clouds, the water mixing ratio should be depleted to about 0.01 times solar at this pressure level. Even though no in situ measurements of the water vapor mixing ratio were made at 1.6 bar, this is consistent with an extrapolation of the increasing water vapor mixing ratio observed at greater pressures, mentioned earlier.

Analysis of Galileo visible images obtained by the Solid State Imager (SSI) identify localized storm systems of violent upwelling, associated with very thick clouds (Banfield et al., 1998; Gierasch et al., 2000). These storm systems occur in horizontal shear zones and appear to be correlated with lightning events seen on the nightside of the planet (Little et al., 1999). Gierasch et al. (2000) conclude that the clouds are most likely composed of water. An other interesting observation is the one by Simon-Miller et al. (2000), who report on the identification of a possible water ice spectral feature around 44 μm in the Voyager IRIS data. They show that this feature is enhanced at certain latitudes on the planet, coinciding with latitudes of postulated convective activity. The water ice particles should be located around 500 mbar, above the ammonia ice cloud, and have a low far-infrared opacity. Roos-Serote et al. (2000) analyzed NIMS spectra of a storm system observed by both SSI and NIMS, within a relatively short timeframe. The NIMS spectra show a high atmospheric water vapor content and significant cloud opacity. Considering the fact that (1) the spatial resolution of NIMS is about 10 times less than SSI, and (2) the thickest clouds are completely opaque to 5-μm radiation, it is apparent that the NIMS data refer to the atmosphere immediately around the storm.

Most previous studies utilizing the Galileo NIMS 5-μm data have been focused on the analysis either of hot spot or storm areas (Irwin et al., 1998, 2001; Nixon et al., 2001; Roos-Serote et al., 1998, 1999, 2000). These areas are not representative of Jupiter as a whole. In this paper we address the question of what can be learned about the global Jovian O/H ratio and the average NEB vertical cloud structure from 5-μm remote sensing observations. We present an analysis of five NIMS spectra from different regions within the NEB, exploring a wide range of possible atmospheric models to constrain these parameters.

First we describe the data, and next the method of analysis. We then discuss general trends, as well as specific findings for each of the individual spectra.

2. NIMS spectra

The Galileo NIMS experiment recorded data cubes (latitude, longitude, wave-length) from many locations of Jupiter over a period of 5 years (1996–2001). NIMS

Table 1
Characteristics of the analyzed spectra (see also Fig. 1a)

Name	Lat. (°)	Lon. (°)	No. of NIMS spectra[d]	Radiance[c] ($\mu W/cm^2/s/\mu m$)	Comments
E4[a] center hs	8.0	319.4	28	62	Center of hot spot
E4[a] border hs	9.4	318.2	33	52	North border of hot spot
C9[b] avneb	9.8	2.7	25	28	Typical warm NEB area
E4[a] west hs	8.3	323.5	33	14	West to hot spot
E4[a] storm	12.9	320.2	66	11	Storm area north to hot spot

[a]E4jnfea53 taken at December 20, 1996 (08:55:37–09:06:25 UT); spatial resolution 340 km/pixel, nightside.
[b]C9jnthrcy107 taken at June 28, 1997 (15:05:23–15:26:48 UT); spatial resolution 350 km/pixel, nightside.
[c]Radiance at 4.9990 μm (E4), 4.9978 μm (C9).
[d]Number of adjacent NIMS spectra used to obtain the average spectrum (see also Fig. 1).

covers a wavelength range of 0.7–5.2 μm, with a relatively low spectral resolving power of 200 at 5 μm (Carlson et al., 1992).

The Jovian thermal infrared spectrum has a window between 4.65 and 5.2 μm, commonly known as the 5-μm window. Due to the low overall atmospheric absorption in this region radiation from pressure levels down to about 8 bar can escape. This is well within the troposphere and below the visible cloud deck, situated between about the 0.5 and 2 bar level. Weak absorption bands from water vapor (dominant for wavelengths larger than 4.8 μm at NIMS spectral resolution), ammonia vapor (towards 5.1 μm, but much weaker than water vapor), as well as phosphine (dominant for wavelengths smaller than 4.7 μm) allow the study of the spatial variation of their abundances (Irwin et al., 1998; Roos-Serote et al., 1998). However, due to the weakness of the features and the low spectral resolution of the NIMS data, no information can be retrieved about the detailed vertical distribution of the species. Rather, the spectra are sensitive to the column abundance in the 3–8 bar region.

Average spectra were extracted from five regions in the NEB, observed on the nightside of the planet, so that pure thermal radiation is measured (Fig. 2a and Table 1). Four spectra were selected from the same NIMS data cube in and around a prominent hot spot in the NEB acquired during Galileo's fourth orbital pass (E4, December 1996). The fifth spectrum was selected from a NIMS observation from orbital pass C9 (June 1997), and is not linked to any particular hot spot. This spectrum can be regarded as an average NEB spectrum. The spectra cover a wide dynamical range of radiances, from very high inside the hot spot (E4 center hs, Table 1), to very low in a cloudy storm area (E4 storm, Table 1). This area has been identified to be related with a thick cloud storm system seen in visible images with the SSI camera (Roos-Serote et al., 2000).

Fig. 1 shows the 5-μm maps of the corresponding areas, as well as the areas that were averaged to obtain the spectra analyzed here. Fig. 2 shows the five spectra and fits using models published previously (Roos-Serote et al., 1998, 1999, 2000), as explained in the next section.

3. Method

The radiative transfer is carried out using a line-by-line code, the same as applied in previous published studies (Roos-Serote et al., 1998, 1999, 2000). This code does not explicitly include scattering by cloud or haze aerosols. Rather, the clouds are given a certain (gray) opacity, and consequently absorb some of the atmospheric radiation travelling up from below. Kirchhof's law is applied to the cloud layers in order to conserve the energy balance. We feel this approach is valid for the data we analyze here, i.e. for the nadir viewing geometry. Roos-Serote et al. (2000) compared a scattering and non-scattering result for the same spectrum, and found similar results. As the cloud particles have strong forward scattering lobes, the effect of scattering in the nadir viewing case is to move peaks of the Contribution Functions (CF) of the radiative transfer equation to lower pressure level. Tests have shown that the difference of the pressure levels of the peaks in the 5-μm window between a scattering and non-scattering atmosphere is of the order of 0.5 bar (Irwin, private communications). This is much less than the FWHM of the CF, which spread over 3 bar.

The new aspect of the present work, relative to previous work performed with this radiative transfer code (Roos-Serote et al., 1998, 1999, 2000), lies entirely in the way the clouds are included in the model atmosphere. We will now very briefly recall the main characteristics of the previous models, as they were used to fit the present data for the purpose of reference. In this paper, we refer to the solar O/H and N/H ratios as given by Anders and Grevesse (1989), unless otherwise stated.

In the model Type 1 (applied in Roos-Serote et al., 1998, 1999, 2000), the temperature profile is fixed to the one measured by the Galileo Probe (Fig. 3(a), Seiff et al., 1996). Table 2 gives the fixed mixing ratios and references of some species included in the calculations. Three parameters were varied:

(1) The (gray) *opacity of a cloud at* 1.55 bar. This cloud has no physical thickness. The cloud level of 1.55 bar

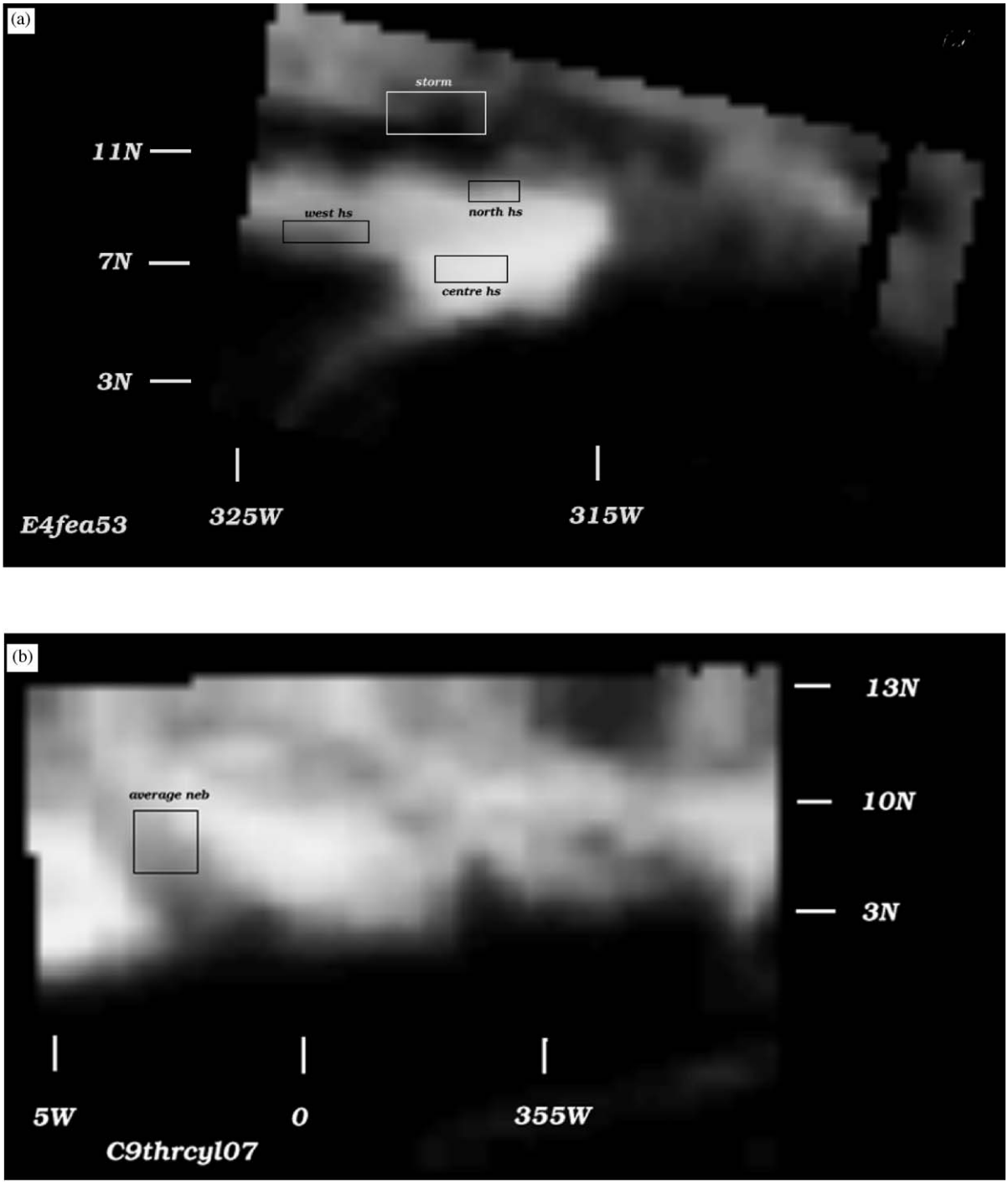

Fig. 1. Maps of E4fea53 and C9thrcyl03 at 5-μm wavelength. The boxes show the areas that were averaged to obtain the five analyzed NIMS spectra (see Table 1).

was chosen in Roos-Serote et al. (1998) based on early analysis of the Galileo Probe nephelometer measurements (Ragent et al., 1996). Later, a more accurate analysis pushed the base of this tenuous cloud to 1.34 bar (Ragent et al., 1998). The change between a thin gray cloud with base at 1.34 or 1.55 bar was found to have a negligible effect on the spectrum in the 5-μm window.

(2) A *saturation factor for water vapor* (Fig. 3(b)). A reference profile, corresponding to the saturation water vapor pressure curve (Atreya, 1986), is multiplied by the saturation factor. This factor essentially gives the relative humidity of the air. At the pressure level where the value of the water vapor mixing ratio equals the deep water vapor mixing ratio, corresponding to the chosen deep O/H ratio, the profile is set constant to this

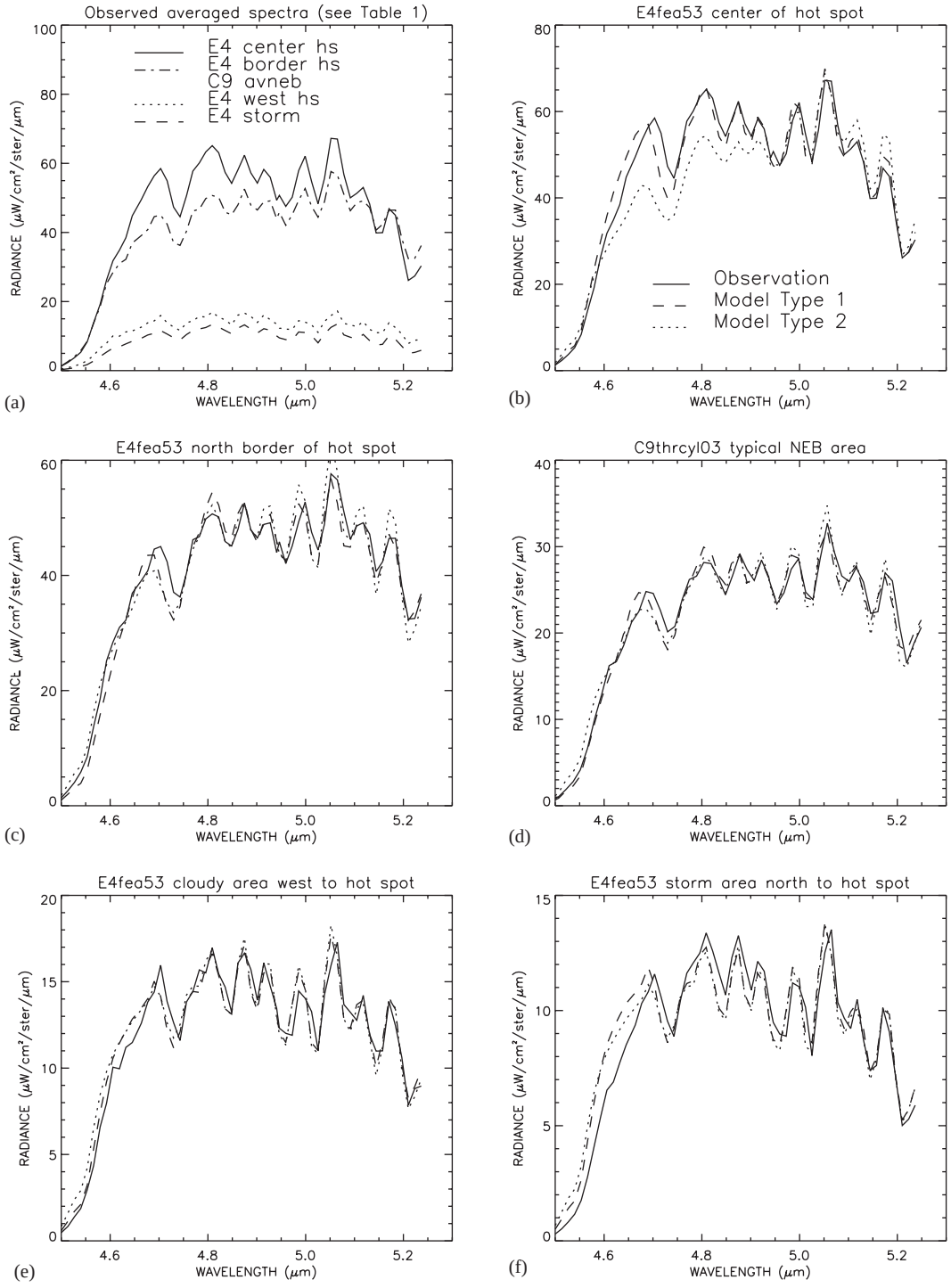

Fig. 2. The five NIMS spectra (Table 1) and the fits from the models Type 1 and Type 2 (see Table 3 for model parameters and the text for explanation).

deep value (see caption of Fig. 3(b) for more details). For example, in the case of a 100% saturated profile and a deep water vapor mixing ratio corresponding to solar O/H, this occurs around 5.1 bar. For a 1% saturated profile, this level descends to 12.8 bar.

(3) A *saturation factor for ammonia vapor* (Fig. 3(c)). An ammonia vapor reference profile was constructed, based on the results from the Galileo Probe Net Flux Radiometer by Sromovsky et al. (1996). Then, similar to the water vapor profile, this reference profile was multiplied with a 'saturation' factor and linked to a constant mixing ratio, corresponding to the chosen deep N/H ratio, in the deep atmosphere at the pressure level where the

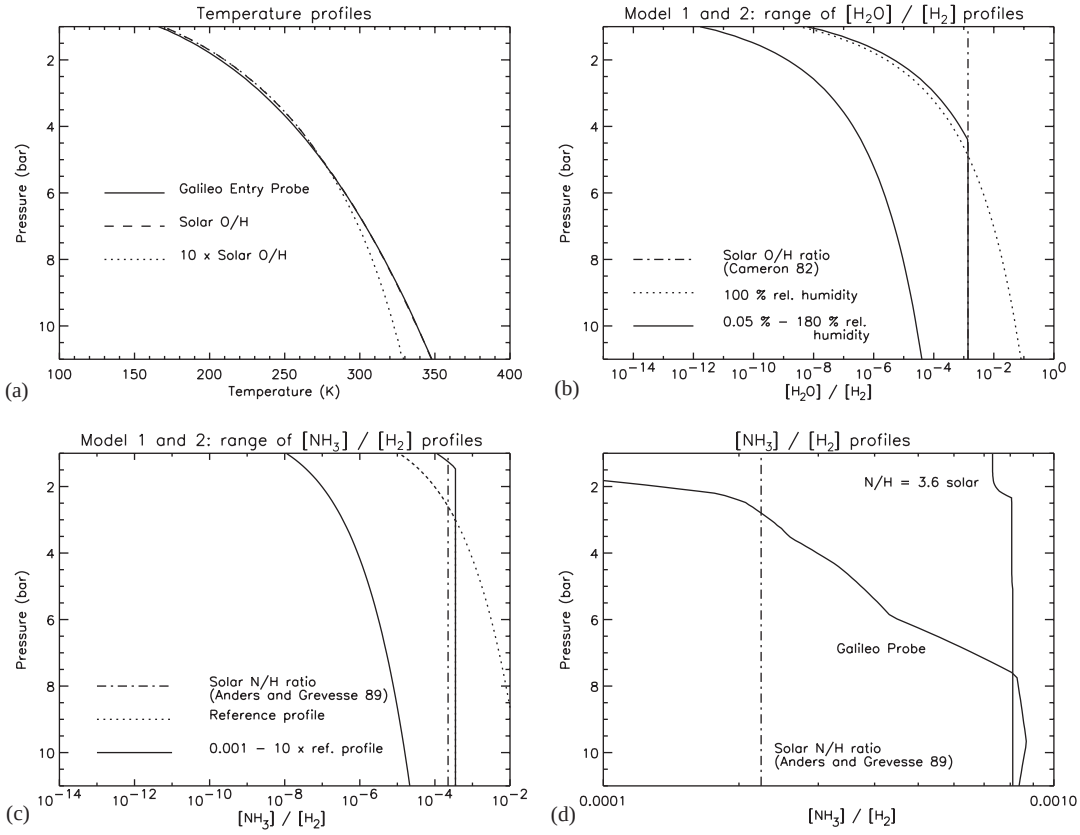

Fig. 3. (a) The Galileo Probe temperature profile, used in models Type 1 and Type 2, and the temperature profiles corresponding to the cases of an atmosphere in thermochemical equilibrium with a deep water vapor mixing ratio of 1.71×10^{-3}, corresponding to 1 times the solar O/H ratio, and 1.71×10^{-2} (10 times solar O/H ratio). (b) The water vapor vertical mixing ratio profiles for models Type 1 and Type 2. In Roos-Serote et al. (1998) the deep atmospheric water vapor mixing ratio (H_2O/H_2) was set to 1.38×10^{-3}, corresponding to the solar O/H value (6.9×10^4) as reported by Cameron (1982). However, the solar elemental ratios are being revised frequently, e.g. $O/H = 8.53 \times 10^{-4}$ in Anders and Grevesse (1989), and as large as 6.5×10^{-4} in Holweger (2001), almost identical to the Cameron (1982) value. (c) The ammonia vapor vertical mixing ratio profiles for models Type 1 and Type 2. The reference profile, adapted from Sromovsky et al. (1996), has $0.01 \times (N/H)_{Sun}$ at 0.5 bar, $0.05 \times (N/H)_{Sun}$ at 1 bar, and $1.6 \times (N/H)_{Sun}$ at 3 bar. Between these levels a log(pressure)–log(mixing ratio) extrapolation was done, and continued for pressures larger than 3 bar. The deep atmospheric ammonia vapor mixing ratio (NH_3/H_2) was set to 3.53×10^{-4} (Sromovsky et al., 1996). This corresponds to 1.6 times the $(N/H)_{Sun}$ value (1.12×10^{-4}) as reported by Anders and Grevesse (1989). Note that the $NH_3/H_2 = 8.1 \times 10^{-4}$ was measured at pressure larger than 8 bar (Folkner et al., 1998). (d) The ammonia vapor vertical mixing ratio profile used in this work, and the profile derived from Galileo Probe data (Atreya et al., 2003; Folkner et al., 1998; Sromovsky et al., 1998).

Table 2
Mixing ratio profiles

X	$[X]/[H_2]$	Comments	Ref.
PH_3	6.944×10^{-7}	Constant	Kunde et al. (1982)
GeH_4	3.000×10^{-10}	Constant	Encrenaz et al. (1996)
CH_3D	2.500×10^{-7}	Constant	Encrenaz et al. (1996)
AsH_3	2.546×10^{-10}	Constant	Noll et al. (1990)
CO	1.852×10^{-9}	Constant	Noll et al. (1988)
CH_4	2.152×10^{-3}	Constant	Niemann et al. (1998)

two are equal (see caption of Fig. 3(c) for more details).

Model Type 2 (applied in Roos-Serote et al., 2000) is the same as model Type 1 with one difference: the inclusion of an extra opaque layer at 5.6 bar. This layer simulates a water cloud expected to form at this level if the deep water vapor mixing ratio equals 2.76×10^{-3} (twice the solar O/H ratio from Cameron (1982) reference used in the previous works, $1.6 \times (O/H)_{Sun}$ for Anders and Grevesse (1989)). As the cloud is set to be opaque, no radiation from below will contribute to the outgoing radiance, so the model atmosphere below the cloud has no influence on the results.

Model Type 1 was used in studies where the emphasis was placed on the analysis of hot spots in the NEB (Roos-Serote et al., 1998, 1999). Due to the high radiance levels, hot spot spectra are of excellent signal-to-noise level. Also, the Galileo Probe made its in situ measurements in such a region, thus providing the best ground-truth to the model calculations (the actual hot spot that the Galileo Probe entered could not be studied by remote sensing). Roos-Serote et al. (2000) analyzed non-hot spot NEB spectra, using both models Type 1 and Type 2. They concluded that for spectra

Table 3
Fit parameters for models Type 1 and Type 2 (see also Fig. 2)

Spectrum	Model 1	Model 2
E4 center hs	$\tau_{cloud} = 0.58$ Water r.h. = 0.9% Ammonia factor =1 $Q = 0.479$	$\tau_{cloud} = 0.22$ Water r.h. = 2% Ammonia factor = 10 $Q = 0.975$
E4 border hs	$\tau_{cloud} = 0.97$ Water r.h. = 0.3% Ammonia factor = 0.001 $Q = 0.405$	$\tau_{cloud} = 0.25$ Water r.h. = 6% Ammonia factor = 0.25 $Q = 0.459$
C9 avneb	$\tau_{cloud} = 1.51$ Water r.h. = 0.4% Ammonia factor = 0.025 $Q = 0.390$	$\tau_{cloud} = 0.82$ Water r.h. = 8% Ammonia factor = 0.25 $Q = 0.427$
E4 west hs	$\tau_{cloud} = 1.61$ Water r.h. = 8% Ammonia factor = 0.1 $Q = 0.461$	$\tau_{cloud} = 1.14$ Water r.h. = 40% Ammonia factor = 0.5 $Q = 0.472$
E4 storm	$\tau_{cloud} = 1.83$ Water r.h. = 8% Ammonia factor = 10 $Q = 0.597$	$\tau_{cloud} = 1.43$ Water r.h. = 40% Ammonia factor = 10 $Q = 0.556$

Note: For model description and discussion see text.

inside a hot spot only models of Type 1 resulted in good fits to the data. This is consistent with the atmospheric structure observed by the Galileo Probe in a hot spot. For spectra outside of hot spots, both models Type 1 and Type 2 result in comparable fits, but with different values for the water vapor abundance and the 1.55 bar cloud opacity: the retrieved amount of water vapor is higher and the 1.55 bar opacity lower in model Type 2 than in model Type 1. This difference is readily explained by considering the CF of the equation of radiative transfer. The CFs peak between 4 and 8 bar with a FWHM of about 3 bar (note that, as a consequence, the 1.55 bar cloud acts as an attenuator of the overall radiance level in the 5-μm window, and does not influence the shape of the spectrum). When placing the opaque layer at 5.6 bar in model Type 2, all contributions from below are blocked. This results in (1) less water vapor absorption (vertical extension of the column is smaller), and (2) alteration of the shape of the spectrum due to the radiation from this cloud layer itself. So, compared to model Type 1, more water vapor is needed in the column to increase the water vapor absorption and shield the radiation from the water cloud. However, more water vapor also affects the overall continuum. To compensate for this, the opacity of the 1.55 bar cloud must be lowered. Figs. 2(b)–(f) show the fits obtained with models Type 1 and Type 2 for the five observed spectra listed in Table 1. Table 3 lists the corresponding fitting parameters. The quality of the fits, quantified by the parameter Q (see Eq. (2) and explanation below), is very similar for both models Type 1 and Type 2, except for the hot spot case.

Now, in the present work, we have treated the model atmosphere in a more realistic and self consistent way. Instead of modeling the clouds as simple layers with no physical thickness, we included results from thermochemical equilibrium cloud models of Atreya et al. (1999). These calculations give the vertical cloud structure (cloud density, ρ_{cloud}, as a function of pressure) for a given deep atmospheric composition. In general three cloud layers form: a water cloud (base at pressures 5–7 bar for $1-3\times(O/H)_{Sun}$), an ammonium hydrosulfide cloud (base between 2 and 2.6 bar) and an ammonia ice cloud (base 0.7–0.85 bar for $1–3\times(N/H)_{Sun}$). The pressure levels of the bases depend on the local composition of the atmosphere. Fig. 4(a) shows an example for an atmosphere with a deep water vapor mixing ratio (H_2O/H_2) of 1.71×10^{-2} (corresponding to a 10 times solar O/H ratio), a deep ammonia vapor mixing ratio of 8.1×10^{-4} (corresponding to 3.6 times solar N/H ratio), as well as a deep mixing ratio of 7.61×10^{-5} for hydrogen sulfide (2.06 times solar S/H). A smaller value for the deep water vapor mixing ratio, and thus the $(O/H)_{Jupiter}$ ratio, results in a water cloud base at lower pressures. Since the amount of cloud condensate at a particular level is mainly a function of temperature, the cloud densities for different models at a given pressure level are similar to each other to within several percent. Table 4 lists the cloud base pressure as a function of the deep $(O/H)_{Jupiter}$ ratio. It should be stressed that the calculated cloud densities represent maximum values, since the thermochemical equilibrium models do not allow for precipitation or dynamical loss of cloud particles.

The ammonia ice cloud lies well above the pressure region where the CFs peak for wavelengths in the 5-μm window, in other words, it lies outside the region where the absorption lines form. The effect of the ammonia ice cloud will be that of attenuating the overall radiance in this window, assuming it is gray. In this study, we excluded the ammonia ice cloud, as its effects will be diluted in the opacity variations of the purported ammonium hydrosulfide cloud.

The transformation of cloud density to cloud opacity as a function of pressure, is obtained by applying the following equation:

$$\tau_{cloud} = \int_{p_1}^{p_2} \mathrm{d}p\, \rho_{cloud}(p) \times \sigma, \tag{1}$$

where τ_{cloud} is the opacity of the cloud between the integration boundaries p_1 and p_2, and $\rho_{cloud}(p)$ is the density of the cloud as a function of pressure from the thermochemical equilibrium calculations. The mass absorption coefficient σ is determined by setting the total opacity of the cloud and perform the integration over the entire atmosphere. This coefficient is assumed not to depend on the wavelength in the 5-μm window. Fig. 4(b) shows a vertical cloud opacity distribution derived from the cloud density distribution presented in Fig. 4(a), and subject to the cloud cutoff pressures as described in the figure caption.

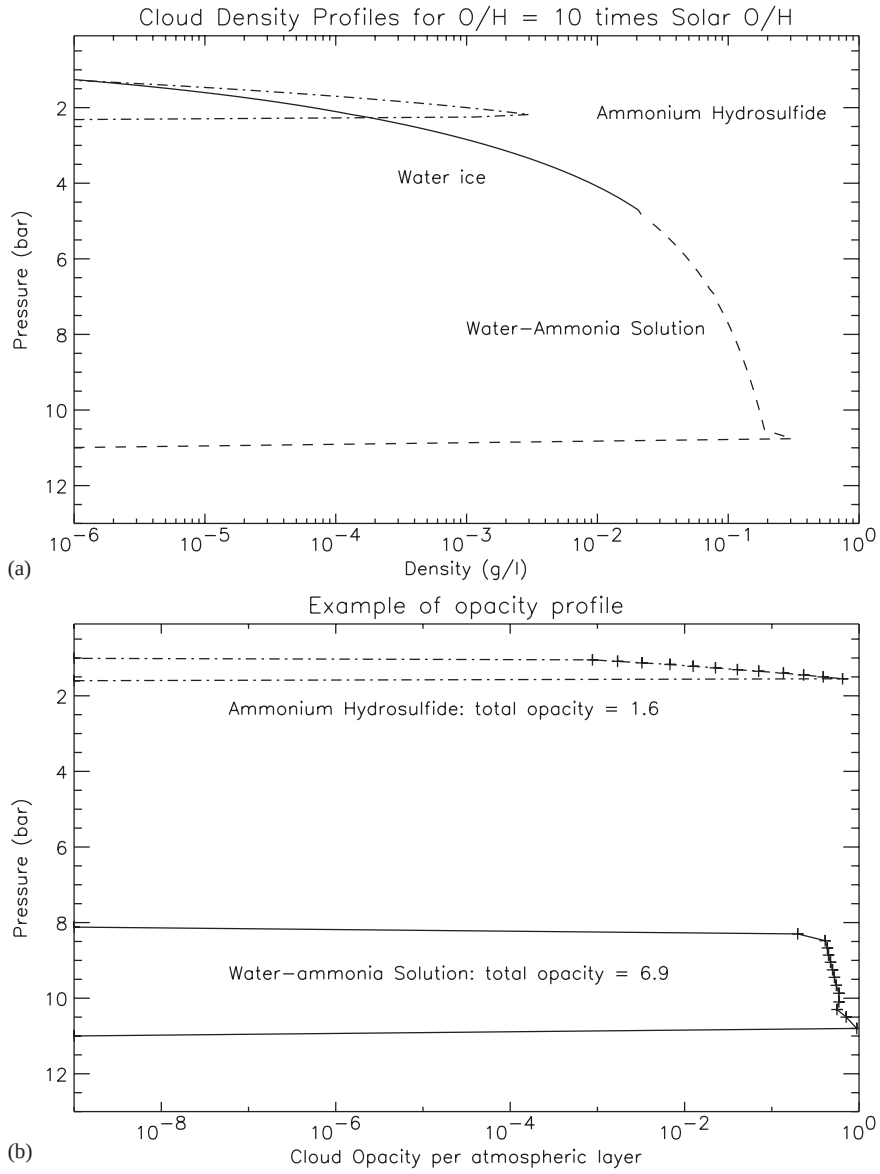

Fig. 4. (a) The cloud density profile for the water cloud in the case of thermochemical equilibrium and a deep water vapor mixing ratio of 1.71×10^{-2}, corresponding to 10 times the solar O/H ratio. The deep ammonia vapor mixing ratio $NH_3/H_2 = 8.1 \times 10^{-4}$, corresponding to 3.6 times solar N/H ratio (constant ammonia mixing ratio profile as in Fig. 3 (d)), and the H_2S mixing ratio is 7.61×10^{-5}, or 2.06 times solar S/H. (b) Example of a vertical cloud opacity distribution derived from the density profiles presented in (a). Here, the cutoff level P_{sub} (see text for explanation) for the water cloud is set to be at 8.12 bar, and the cloud saturation to zero, i.e. no cloud opacity at pressures smaller then 8.12 bar. The total water cloud opacity is set to 6.9, a value chosen for practical reasons in the radiative transfer model. The total ammonium hydrosulfide cloud opacity is set to 1.6, and the cloud base is lifted to 1.55 bar by cutting off the cloud density profile at higher pressures. The cutoff at 1 bar of this cloud is where the model atmosphere stops, as both atmospheric and cloud emission at pressure smaller than 1 bar have a negligible contribution to the radiance in the 5-μm window.

Table 4
Cloud parameters for model parameters

$\frac{O/H_{Jupiter}}{O/H_{Sun}}$ [a]	$[H_2O]/[H_2]_{deep}$	$P_{watercloudbase}$ (bar)
0.3	5.13×10^{-4}	4.10
1.0	1.71×10^{-3}	4.98
2.0	3.42×10^{-3}	6.02
3.0	5.13×10^{-3}	6.81
5.0	8.55×10^{-3}	7.97
10.0	1.71×10^{-2}	10.80

[a] $(O/H)_{Sun} = 8.53 \times 10^{-4}$ from Anders and Grevesse (1989).

A set of six free parameters specifies each atmospheric model:

(1) The $(O/H)_{Jupiter}$ ratio in the deep well-mixed atmosphere taken 0.3, 1, 2, 5, and 10 × $(O/H)_{Sun}$ (see Table 4) (8.53×10^{-4} from Anders and Grevesse, 1989).
(2) The total opacity of the ammonium hydrosulfide cloud, with a cloud base at 2.27 bar in the case of a deep $[NH_3]/[H_2] = 8.1 \times 10^{-4}$, i.e. $3.6 \times (N/H)_{Sun}$ (Anders and Grevesse, 1989; Folkner et al., 1998).

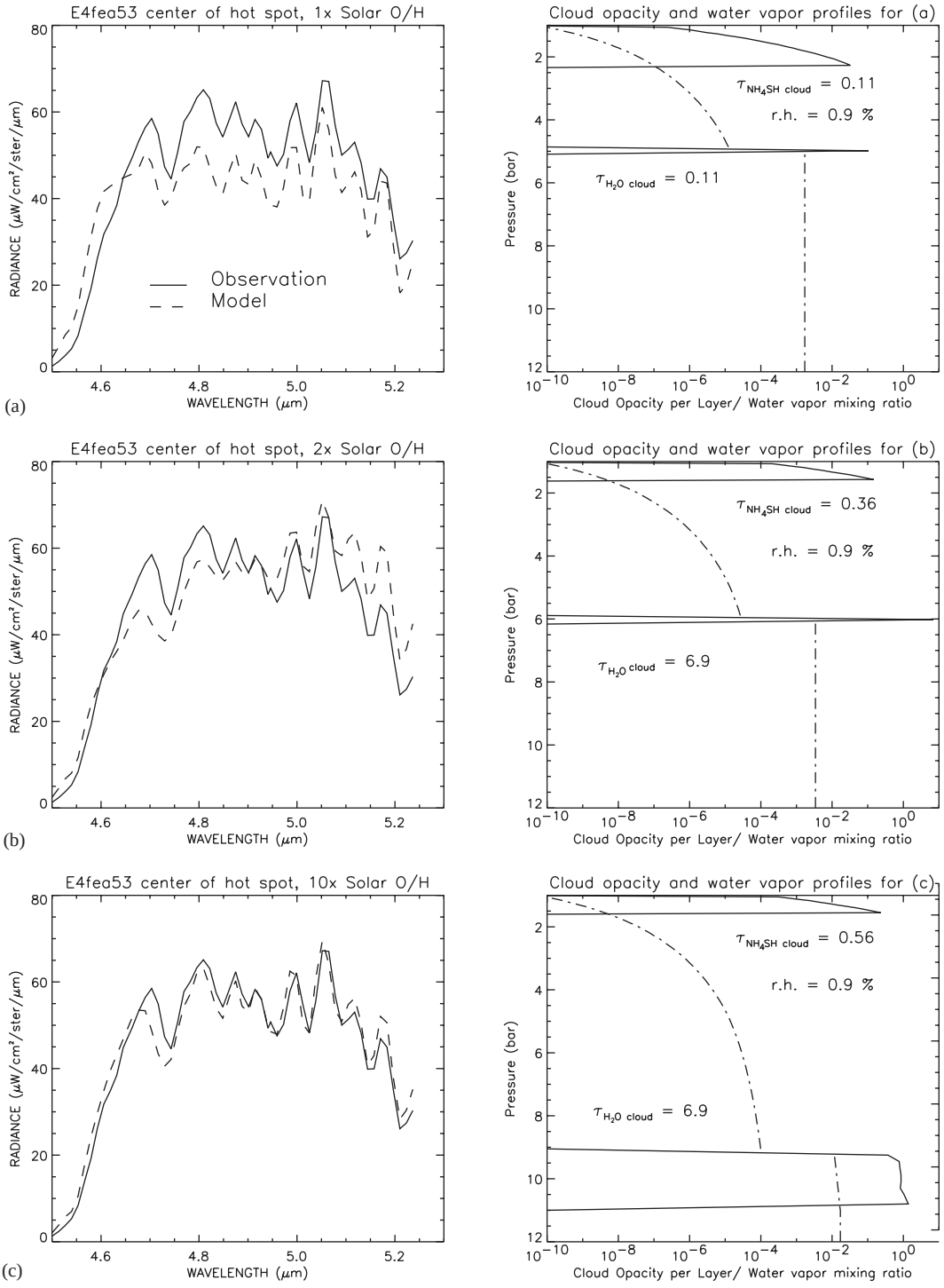

Fig. 5. Selected fits to the spectrum from E4 center of the hot spot (Table 1). See Table 5 for the model parameters of the fits, and the text for detailed discussion.

(3) The total opacity of the water (liquid + ice) cloud.
(4) A subsaturation pressure level, P_{sub}.
(5) The relative humidity of water vapor for pressures smaller than P_{sub}, i.e. a factor of multiplication applied to the saturated water vapor profile at these pressures (see Figs. 5–9 for examples of the water vapor profiles). The relative humidity inside the water cloud is always kept at 100%.
(6) The factor of multiplication for the water cloud density profile, applied for pressures smaller than P_{sub}.

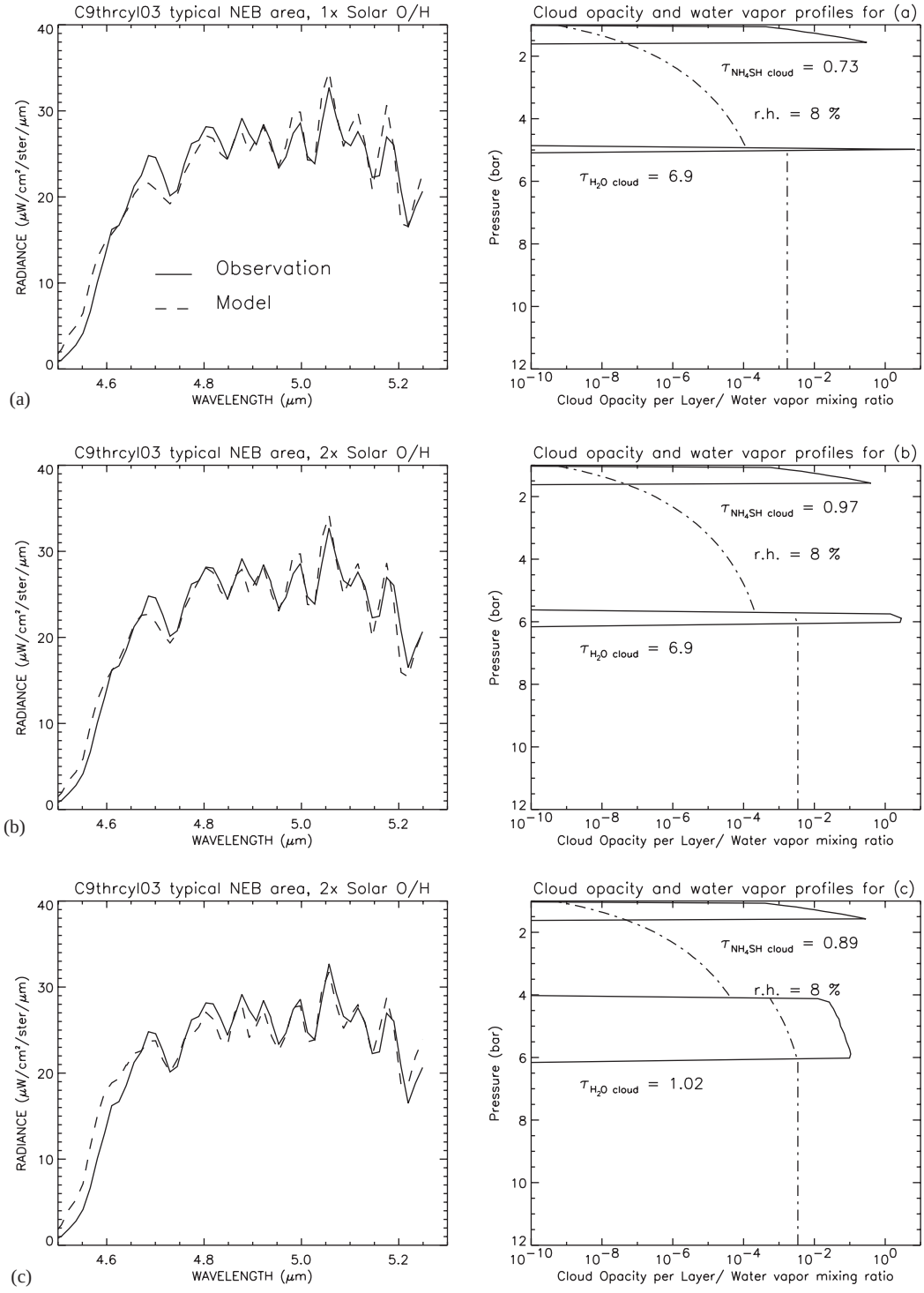

Fig. 6. Selected fits to the spectrum from C9, a typical NEB region (Table 1). See Table 5 for the model parameters of the fits, and the text for detailed discussion.

Other parameters are kept constant (see Table 2). These six parameters are not independent, for example, setting the cloud structure restricts the possible relative humidity. We did not try to determine any explicit dependences. Initially, the ammonia vapor vertical mixing ratio profile was kept the same for all calculations, i.e. a constant profile ($[NH_3]/[H_2] = 8.1 \times 10^{-4}$) upto the ammonium hydrosulfide cloud base (Fig. 3(d)). Later, different ammonia vapor profiles were tested, in particular the one presented in Atreya et al. (2003), combined from results from Galileo Probe

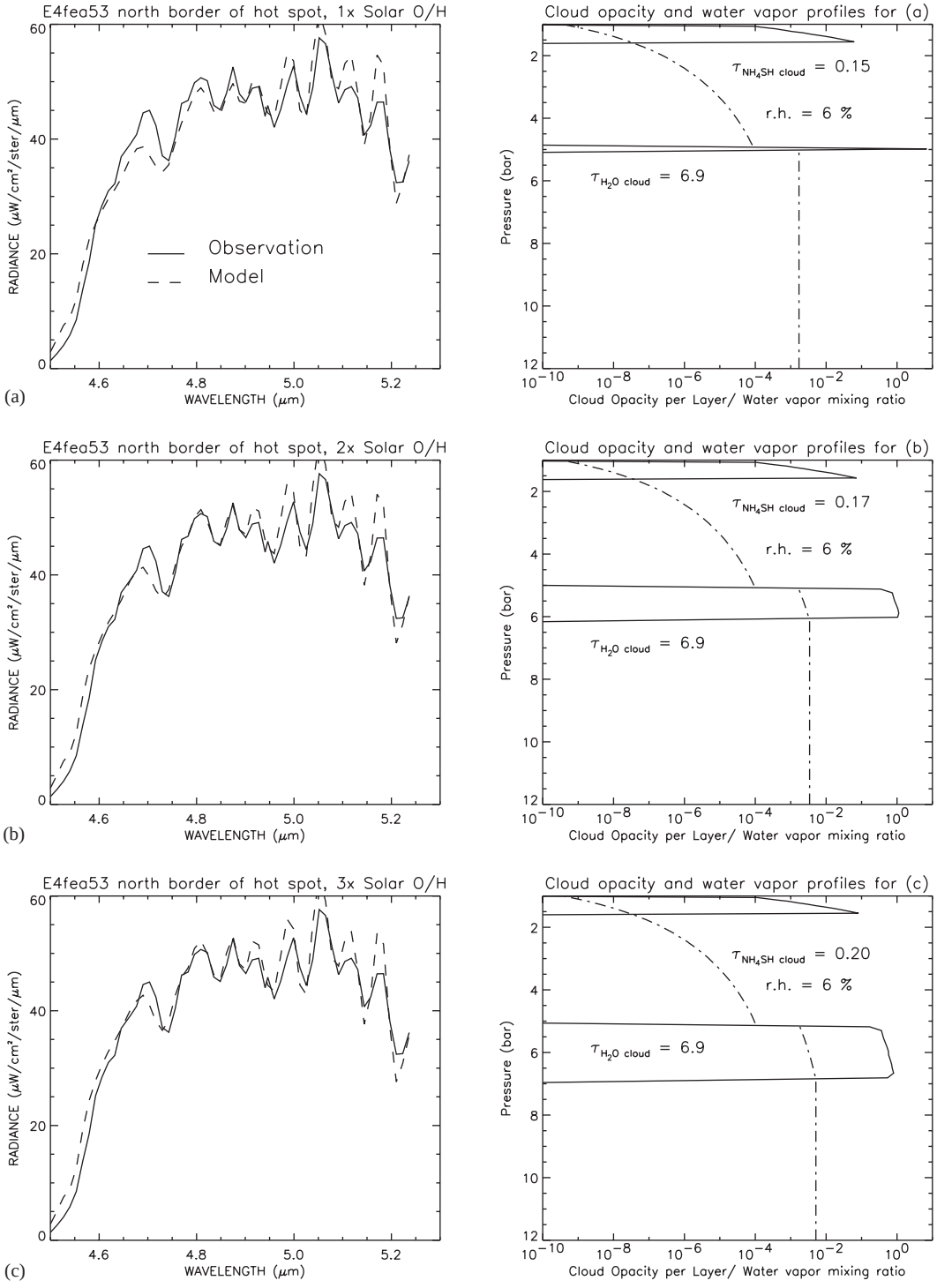

Fig. 7. Selected fits to the spectrum from E4 at the north border of the hot spot (Table 1). See Table 5 for the model parameters of the fits, and the text for detailed discussion.

measurements (Sromovsky et al., 1998; Folkner et al., 1998; see also Fig. 3(d)). Temperature profiles also change slightly from one (O/H ratio) model to the other due to the release of latent heat from the condensation of the water cloud. Fig. 3(a) compares the applied temperature profiles for the different cases of Table 4.

4. Results and discussion

Extensive tests were performed on each of the five spectra listed in Table 1. For every $(O/H)_{Jupiter}$ ratio (Table 4) the best fit to the observed spectrum was found by adjusting the values of parameters (2)–(6). In this process, parameters

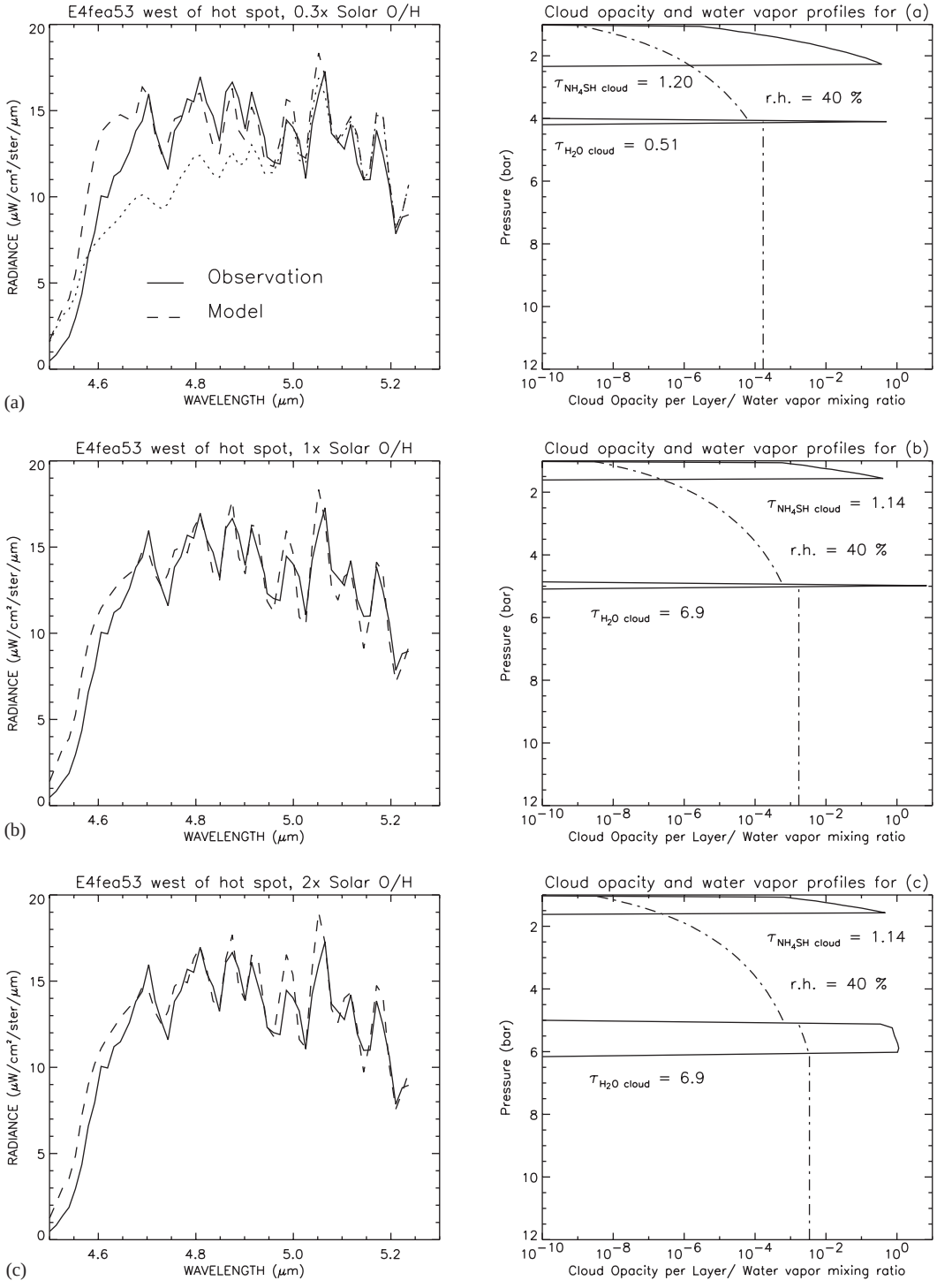

Fig. 8. Selected fits to the spectrum from E4 west of the hot spot (Table 1). See Table 5 for the model parameters of the fits, and the text for detailed discussion.

(3)–(6) were set to different fixed values, and parameter (2) was modified to obtain the best fit. The quality of the fit was determined from;

$$Q^2 = \sum_{\lambda} \left(\frac{I_{\lambda}^{\mathrm{obs}} - I_{\lambda}^{\mathrm{syn}}}{I_{\lambda}^{\mathrm{obs}}} \right)^2, \qquad (2)$$

where $I_{\lambda}^{\mathrm{obs}}$ and $I_{\lambda}^{\mathrm{syn}}$ are the observed and synthetic spectral radiances at wavelength λ. The sum was taken over 48 wavelengths (NIMS detectors 16 and 17, Carlson et al., 1992) between 4.65 and 5.2 μm. The goodness of the fits produced in this work was based on the minimum value of Q coupled with a visual evaluation. Note that the noise at a given

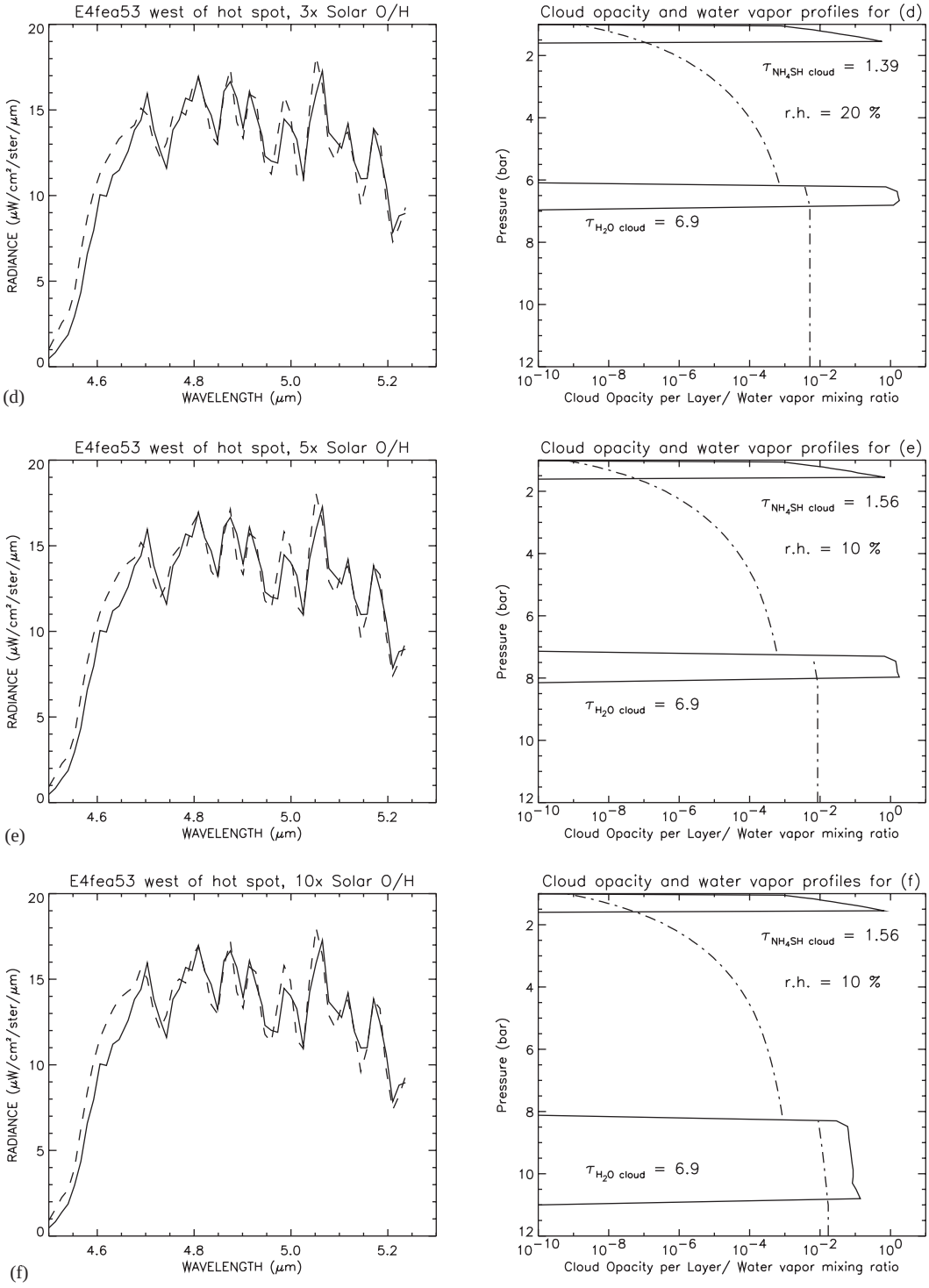

Fig. 8. *continued.*

wavelength is of the order of 5% of the radiance as found by Nixon et al. (2001). In order for a fit to be within the noise, Q should be smaller than 0.346 for 48 wavelenghts. However, even the best fits always stay above this level. It is known that the model gives accurate fits to very high spectral resolution Jupiter data (FTS spectra with $R = 12,000$, see Roos-Serote, 1997). So we believe this discrepency is due to systematic unaccounted for uncertainties in the wavelength calibration and spectral response function, and/or radiometric calibration of the NIMS experiment.

In Figs. 5–9 we show representative examples of fits to each individual spectrum. Table 5 lists the parameters of

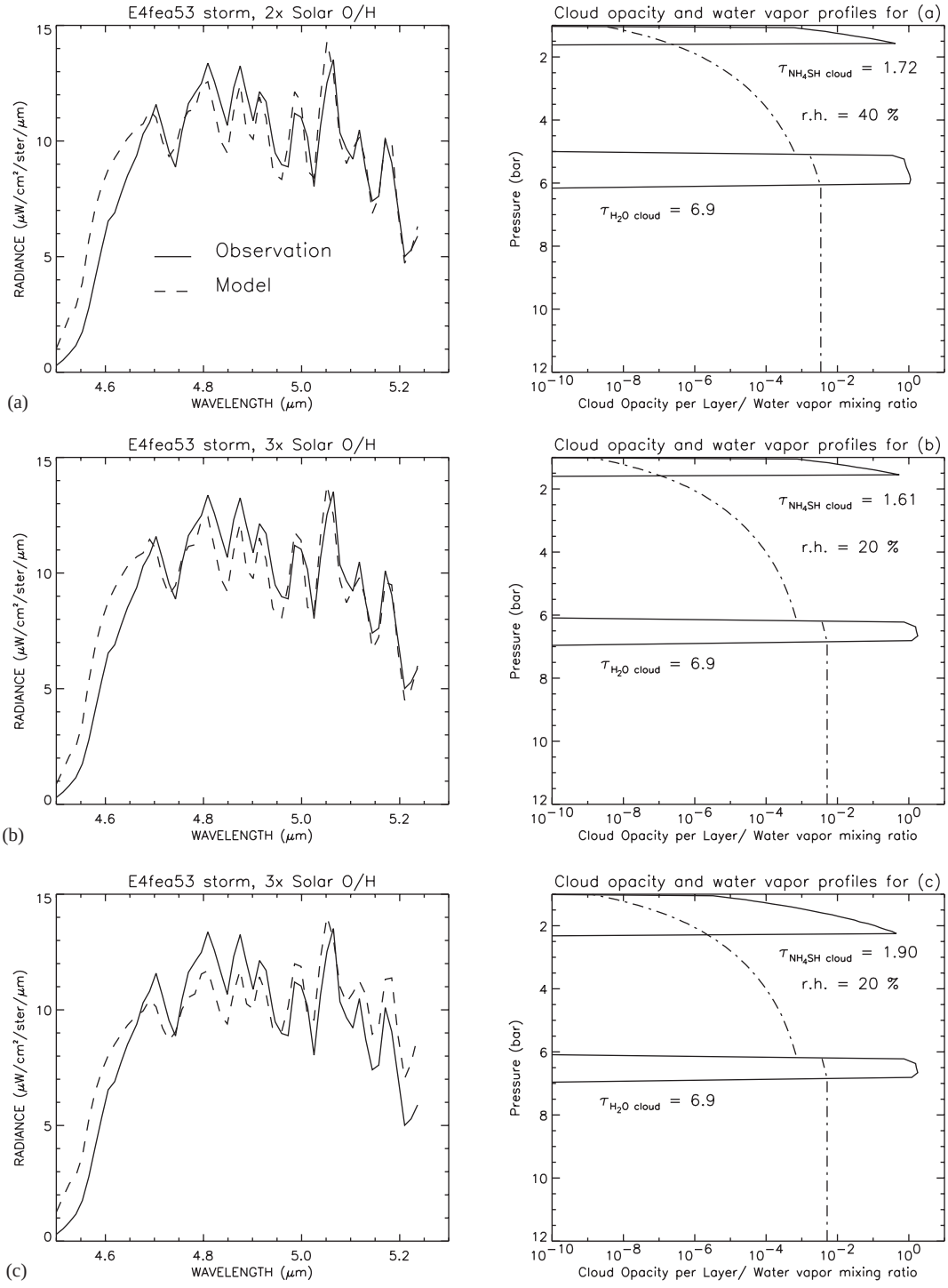

Fig. 9. Selected fits to the spectrum from E4 storm system (Table 1). See Table 5 for the model parameters of the fits, and the text for detailed discussion.

the corresponding models. Considering the entire set of fits (several hundreds of models), we noticed three important general trends. These are the main findings of this work.

(1) The model for $(O/H)_{Jupiter} = 0.3 \times (O/H)_{Sun}$ has a water cloud base at 4.1 bar. None of the spectra can be satisfactorily fit with this model. Two examples are shown in Fig. 8(a) for the E4 west spectrum (see Table 5). This model can be excluded safely.

(2) Even more constraining than the previous point, we find that in order to fit any of the spectra, no *significant* cloud opacity in the region of pressures between about 2.5 and 5 bar is allowed. For some cases, we found that some opacity is allowed for pressures be-

Table 5
Model parameters for the fits shown in Figs. 5–9

Spectrum[a]	$\frac{O/H_{Jupiter}}{O/H_{Sun}}$ [b,c]	$\tau_{H_2Ocloud}$	P_{sub}[d] (bar)	Rel. humidity. (%)	$\tau_{NH_4SHcloud}$	NH_3 profile[e]	Q[f]
E4 center hs							
(Fig. 5a)	1.0	0.11	4.86	0.9	0.11	2	1.283
(Fig. 5b)	2.0	6.9	5.89	0.9	0.36	2	1.179
(Fig. 5c)	10	6.9	9.05	0.9	0.56	2	0.538
C9 avneb							
(Fig. 6a)	1.0	6.9	4.86	8	0.73	2	0.478
(Fig. 6b)	2.0	6.9	5.62	8	0.97	2	0.412
(Fig. 6c)	2.0	1.02	4.00	8	0.89	2	0.370
E4 north hs							
(Fig. 7a)	1.0	6.9	4.86	6	0.15	2	0.502
(Fig. 7b)	2.0	6.9	5.00	6	0.17	2	0.449
(Fig. 7c)	3.0	6.9	5.06	6	0.20	2	0.446
E4 west hs							
(Fig. 8a)	0.3	0.51	4.00	40	1.20	1	0.644
(Fig. 8a)	0.3	6.9	4.00	40	1.20	1	1.244
(Fig. 8b)	1.0	6.9	4.86	40	1.14	2	0.520
(Fig. 8c)	2.0	6.9	5.00	40	1.14	2	0.528
(Fig. 8d)	3.0	6.9	6.09	20	1.39	2	0.497
(Fig. 8e)	5.0	6.9	7.14	10	1.56	2	0.483
(Fig. 8f)	10	6.9	8.12	10	1.56	2	0.507
E4 storm hs							
(Fig. 9a)	2.0	6.9	5.00	40	1.72	1	0.595
(Fig. 9b)	3.0	6.9	5.02	20	1.61	1	0.671
(Fig. 9c)	3.0	6.9	5.02	20	1.90	1	1.156

[a]See Table 1 for the description of the spectra.
[b]See Table 4 for the water cloud base levels of each model.
[c]$(O/H)_{Sun} = 8.53 \times 10^{-4}$ from Anders and Grevesse (1989).
[d]All models presented here have zero cloud opacity for pressures smaller than P_{sub}.
[e]NH_3 profiles: (1) constant corresponding to $(N/H)_{Jupiter}$ ratio of 3.6 times the solar value, and (2) Galileo Probe profile (see Fig. 3(d)).
[f]Q defined in Eq. (2) compare to best results from models Type 1 and Type 2 (Table 3).

tween 4 and 5 bar, but it is always a small amount ($\ll 1$). The bulk of the opacity is located at pressures greater than 5 bar (p.e. Fig. 6(c)). This means that when $(O/H)_{Jupiter}$ equals $(O/H)_{Sun}$, and the water cloud base forms at 4.98 bar, the cloud should be either vertically very thin (of the order of 0.1 bar) or, if it extends to lower pressures, very tenuous. In the case of higher $(O/H)_{Jupiter}$ ratios, where the water cloud bases are located deeper in the atmosphere (Table 4), the water cloud tops should not exceed the 5 bar pressure level.

These two observations contain the main findings of this work. The result is not unique however. As shown in Fig. 2(b)–(f), the same spectra can also be fit using a model *without* any water clouds in the observable part of the atmosphere. In this case the O/H ratio in the observable part of the atmosphere is less than solar.

Yet, we believe the presence of water clouds in the atmosphere of Jupiter at pressures greater than 4–5 bar to be plausible, based on the results of our calculations and the results from previous work that show that (1) localized thick clouds, probably composed of water vapor, are related to lightning events and strong vertical convection (Banfield et al., 1998; Gierasch et al., 2000; Little et al., 1999; Roos-Serote et al., 2000), (2) high thin water ice clouds are found at the same latitudes as the strong convective events (Simon-Miller et al., 2000), and that (3) the dryness and the absence of clouds in 5-μm hot spots can be explained by dynamics (Showman and Dowling, 2000).

The restriction that the cloud base should be placed at pressures greater than 5 bar implies a lower limit on the $(O/H)_{Jupiter}$ ratio of at least the $(O/H)_{Sun}$. Better constraints on results on the O/H ratio as determined from remote sensing data will be possible upon availability of a detailed vertical structure of the Jovian clouds from future observations.

Due to the limited spectral resolution of the NIMS experiment, which results in a limited sensitivity to vertical opacity distribution, it is not possible to distinguish between, for example, a model with

$(O/H)_{Jupiter} = 3 \times (O/H)_{Sun}$ and $(O/H)_{Jupiter} = 5 \times (O/H)_{Sun}$. Furthermore, it is important to note that these results are valid for the NIMS spatial resolution, which is on the order of 350 km/pixel at best for most of Jupiter atmospheric observations. The atmospheric structure is heterogeneous at small spatial scales, in particular as observed by the Galileo SSI experiment, which has an order of magnitude better spatial resolution (Banfield et al., 1998; Gierasch et al., 2000).

(3) The NIMS 5-μm spectrum is not as sensitive to variations in the ammonia vapor mixing ratio as it is to variations in the water vapor mixing ratio. Yet, some trends could be identified. We performed a series of tests, in which we changed the ammonia vertical mixing ratio profile and the ammonium hydrosulfide cloud base pressure. If the deep $N/H_{Jupiter}$ ratio is 3.6 times the solar value, the ammonium hydrosulfide cloud forms at around 2.27 bar (Fig. 3(d)). A change of just this pressure to 2 bar, does not have a big effect on the synthetic spectrum. A change to smaller pressures than 2 bar has a significant effect on the slope of the spectrum in the 4.65–5.2 μm region, i.e. it becomes more negative as the cloud base pressure decreases. This is exemplified in Fig. 9(b) and (c) for the E4 storm spectrum, but is valid for all other spectra as well. We also find that we can obtain better fits if we take a cloud base at pressures less than 2 bar and a different ammonia profile, i.e. with less ammonia at the cloud formation level. We used the Galileo Probe ammonia vapor profile, which shows a depleted abundance of ammonia in the upper troposphere (see Fig. 3(d)). This correlation between the ammonia mixing ratio and the cloud base pressure is expected from thermodynamic considerations. We found this effect to be true for all spectra, except for the E4 storm spectrum (see the discussion of the individual spectra below).

We conclude that in the NEB, the purported ammonium hydrosulfide cloud base is located at pressures between about 1.3 and 1.6 bar, with a depleted ammonia vapor mixing ratio. In this context, it is interesting to notice that Irwin et al. (2001), from a comparison of visible and near-infrared SSI and NIMS data, conclude that the variation of 5-μm brightness in the NEB is best explained by cloud opacity variations in the 1–2 bar region.

We now discuss some particular features of the individual spectra (Figs 5–9 and Table 5).

4.1. E4 hot spot center (Fig. 5)

This is a spectrum from the E4 hot spot, a region extensively analyzed in previous works by Roos-Serote et al. (1998, 2000). No new surprises were found, i.e. dry atmosphere (relative humidity $\sim$ 1%), no water cloud at pressures smaller than 8 bar (Fig. 5(a)–(c)), and a low ammonium hydrosulfide cloud opacity (< 0.5), located between 1.3 and 1.6 bar, with depleted ammonia (Fig. 3(d)). These results are entirely in agreement with the in situ Galileo Probe measurements of another hot spot area.

4.2. C9 regular NEB (Fig. 6)

This is an average NEB area, not close to any hot spot, observed on the nightside of Jupiter. We find a water vapor content corresponding to about 10% relative humidity, and an opacity of about 1 for the ammonium hydrosulfide cloud, with a base located between 1.3 and 1.6 bar. For the water cloud different models are possible. Some extension of the cloud up to the 4 bar level is allowed, under the condition that the total opacity of the cloud between 4 and 5 bar is much smaller than unity (Fig. 6(b) and (c)).

4.3. E4 hot spot north border (Fig. 7)

This area is at the north border of the E4 hot spot, a transition between the hot spot and a more typical NEB area. The inferred water vapor relative humidity is about 5–6%, in between that of the hot spot and the average NEB. The water cloud tops cannot extend above the 5 bar level. As 5% relative humidity in water vapor does result in significant absorption of the overall 5-μm window radiation, the opacity of the ammonium hydrosulfide cloud is found to be small, i.e. on the order of 0.2. Fig. 7(a)–(c) show a sequence of models with increasing $(O/H)_{Jupiter}$. In the case of a water cloud free atmosphere (model Type 1, see Fig. 2(c) and Table 3) the water vapor mixing ratio is an order of magnitude less, and the ammonium hydrosulfide cloud opacity about unity. All cases have a similar value of Q. This is a good example of the non-uniqueness of the problem of fitting the data and determining the structure of the atmosphere.

4.4. E4 West of hot spot (Fig. 8)

For this area we unexpectedly find a high water vapor content, i.e. between 10 and 40% relative humidity, depending on the chosen cloud model. We show the best fit for all six different values of the $(O/H)_{Jupiter}$ ratio from Table 4. Fig. 8(a) shows the case of an $(O/H)_{Jupiter}$ ratio 0.3 times the $(O/H)_{Sun}$, where the water cloud base is at 4 bar. The figure shows the calculations for a thin opaque water cloud (dotted line) and a thin transparent water cloud (dashed line). Both models are clearly inconsistent with the data, conclusion valid for the other spectra as well. The model with the depleted ammonia abundance profile and a ammonium hydrosulfide cloud with a base between 1.3 and 1.6 bar, is only slightly better than the non-depleted ammonia abundance profile (Fig. 3(d)). The total opacity of the ammonium hydrosulfide cloud is between 1 and 2. In images at visible wavelengths the area does not show any evidence of active meteorology like violent upwelling and the formation of very thick clouds. It is perhaps related to the wave

phenomenon that forms the hot spots (Friedson and Orton, 1999; Baines et al., 2002). The hot spots being the downwelling part of the wave, the region west of the hot spot would correspond to the upwelling part, bringing up humid Jovian air from deeper down. The inferred water vapor mixing ratio (larger than about 10–20%) may be representative of its value in the deep well-mixed atmosphere.

4.5. E4 Storm (Fig. 9)

This spectrum is in the area where at visible wavelengths a thick storm cloud is seen, extending to high altitudes (Roos-Serote et al., 2000; Gierasch and Banfield, priv. comm.) Clouds of this type seen in other observations and locations have been found to be related to lightning events (Little et al., 1999). We find that the NIMS spectra are consistent with a high atmospheric water vapor content, i.e. 20–100% relative humidity. Still, no significant water cloud opacity is allowed at pressures smaller than 5 bar. It should be stressed that NIMS does not see the storm itself, because the cloud is so thick that no significant 5-μm thermal radiation escapes from below, and the cloud tops are high and cold. The spatial resolution of the NIMS data is another limiting factor, as the size of the core of the storm system is of the order of several NIMS pixels. Rather, NIMS observes the less cloudy areas in the immediate neighbourhood of the storm. In contrast with the results from the other spectra, for this spectrum a constant ammonia mixing ratio profile gives the best results, if combined with an ammonium hydrosulfide cloud base at 1.5 bar (Fig. 9(a)–(c)). For this ammonia profile, the base of the purported NH_4SH cloud is expected to be at 2.27 bar. This effect is shown in Fig. 9(b) and (c) (see Table 5 for model parameters). A speculative qualitative explanation may be the following: humid air (water and ammonia) is drawn in from the areas around the strong and localized upwelling cloud towers, at pressures below the tower bases (higher than 3 bar). Dried air downwelling from above and next to the towers mixes with the wetter air down to, at least, the level where the ammonium hydrosulfide cloud will form. As a result, the base of this cloud forms at lower pressures, and the cloud is not very opaque, making it possible for NIMS to observe the wetter air below.

5. Conclusions

The goal of the present study is to investigate what can be learned about the global Jovian O/H ratio and vertical NEB cloud structure from Galileo NIMS 5-μm remote sensing data. No firm conclusions can be made on either of these quantities due to the non-uniqueness of the problem of modelling these data. Yet, some constraints can be obtained. Except for the hot spot regions, all the regions studied in this work can be represented by two types of models, i.e. the spectra can be fitted equally well with two different model atmospheres. One of the scenarios is an atmosphere with no clouds between the 2.5 and 8 bar region of the atmosphere, sounded in the 5-μm part of the spectrum. In this scenario the water vapor mixing ratio down to 8 bar is never greater than about 10% of relative humidity, which corresponds to a $(O/H)_{Jupiter}$ ratio much less than the $(O/H)_{Sun}$ ratio throughout this part of the atmosphere. In the other scenario, we include clouds predicted by thermochemical equilibrium calculations for a given composition of the atmosphere. In this case, the data can be fit by synthetic spectra calculated with model atmospheres where a water cloud forms at 5 bar or higher pressures, i.e. the $(O/H)_{Jupiter}$ ratio is equal to or higher than the $(O/H)_{Sun}$ ratio. The relative humidities can go up to 100% in the observable part of the atmosphere. Models where either the clouds form in the 2.5–5 bar region, which happens when $(O/H)_{Jupiter}$ is less than $(O/H)_{Sun}$, or where the clouds extend into this region and have significant opacity, can be excluded, as they result in synthetic spectra that are incompatible with the data. Cloud precipitation or dynamical loss could indeed clear out the air of thick clouds, but our required cut off at 5 bar seems somewhat artificial and remains to be explained. Finally, we find that the depleted ammonia profile measured in situ by the Galileo Probe, combined with the formation of the purported ammonium hydrosulfide cloud at pressures between 1.3 and 1.6 bar, results in better fits to most of the data. Only the areas expected to be related to strong vertical upwelling show higher ammonia mixing ratio values. When, in the future, independent measurements of the deep vertical cloud structure will become available either from remote sensing techniques and data analysis or from new in situ measurements, then it will be possible to discriminate between atmospheric models, and to better constrain the Jovian O/H ratio. Eventually, we will learn more about how this and other giant planets formed and evolved.

Acknowledgements

MRS acknowledges support from a project /ESO/PRO/15131/1999 financed by the Portuguese Foundation for Science and Technology (FCT), and from research fellowship of the University of Michigan between September and December, 2000. SKA's research was supported by NASA's Planetary Atmospheres Program.

References

Anders, E., Grevesse, N., 1989. Abundances of the elements: meteoritic and solar. Geochim. Cosmochim. Acta 53, 197–214.

Atreya, S.K., 1986. In: Atmospheres and Ionospheres of the Outer Planets and their Satellites. Springer, New York, Berlin, p. 56.

Atreya, S.K., Romani, P., 1985. In: Hunt, G.E. (Ed.), Planetary Meteorology. Cambridge University Press, Cambridge, pp. 17–68.

Atreya, S.K., Wong, M.H., Owen, T.C., Mahaffy, P.R., Niemann, H.B., de Pater, I., Drossart, P., Encrenaz, T., 1999. A comparison of the atmospheres of Jupiter and Saturn: deep atmospheric composition,

cloud structure, vertical mixing, and origin. Planet. Space Sci. 47, 1243–1262.

Atreya, S.K., Mahaffy, P.R., Niemann, H.B., Wong, M.H., Owen, T.C., 2003. Composition and origin of the atmosphere of Jupiter—an update, and implications for the extrasolar giant planets. Planet. Space Sci. 51, 105–112.

Baines, K.H., Carlson, R.W, Kamp, L.W., 2002. Fresh ammonia ice clouds in Jupiter. Icarus 159, 74–94.

Banfield, D., Gierasch, P.J., Bell, M., Ustinov, E., Ingersoll, A.P., Vasavada, A.R., West, R.A., Belton, M.J.S., 1998. Jupiter's cloud structure from Galileo imaging data. Icarus 135, 230–250.

Bjoraker, G.L., Larson, H.P., Kunde, V., 1986. The abundance and distribution of water vapor in Jupiter's atmosphere. Astrophys. J. 311, 1058–1072.

Bjoraker, G.L., Hewagama, T., Orton, G.S., 2002. Evidence for water clouds on Jupiter from 5, micron spectra. Bull. Am. Astron. Soc. 34, 874.

Cameron, A.G.W., 1982. Elemental and nuclide abundances in the solar system. In: Barnes, C.A., Clayton, D.D., Schramm, D.N. (Eds.), Essays in Nuclear Astrophysics. Cambridge University Press, Cambridge, England, pp. 23–46.

Carlson, R.W., Weissman, P.R., Smythe, W.D., Mahoney, J.C., 1992. the NIMS Science and Engineering Team, Near-infrared mapping spectromenter experiment on Galileo. Space Sci. Rev. 60, 457–460.

Drossart, P., Encrenaz, Th., 1982. The abundance of water on Jupiter from the Voyager/IRIS data at 5 μm. Icarus 52, 483–491.

Encrenaz, Th., de Graauw, Th., Schaeidt, S., Lellouch, E., Feuchtgruber, H., Beintema, D.A., Bézard, B., Drossart, P., Griffin, M., Heras, A., Kessler, M., Leech, K., Morris, A., Roelfsema, P.R., Roos-Serote, M., Salama, A., Vanden-bussche, B., Valentijn, E.A., Davis, G.R., Naylor, D.A., 1996. First results of ISO–SWS observations of Jupiter. Astron. Astrophys. 315, L397–L400.

Folkner, W.M., Woo, R., Nandi, S., 1998. Ammonia abundance in Jupiter's atmosphere derived from attenuation of the Galileo probe's radio signal. J. Geophys. Res. 103, 22,847–22,856.

Friedson, A.J., Orton, G.S., 1999. A dynamical model of Jupiter's 5-micron hot spots. Bull. Am. Astron. Soc. 31, 1155–1156.

Gautier, D., Hersant, F., Mousis, O., Lunine, J.L., 2001a. Enrichment in volatiles in Jupiter: a new interpretation of the *Galileo* measurements. Astrophys. J. 550, L227–L230.

Gautier, D., Hersant, F., Mousis, O., Lunine, J.L., 2001b. Erratum: Enrichment in volatiles in Jupiter: a new interpretation of the *Galileo* measurements. Astrophys. J. 559, L183.

Gierasch, P., Ingersoll, A.P., Banfield, D., Ewald, S.P., Helfenstein, P., Simon-Miller, A., Vasavada, A., Breneman, H.H., Senske, D.A., 2000. the Galileo Imaging Team, Observation of moist convection in Jupiter's atmosphere. Nature 403, 628–630.

Hanel, R., Conrath, B., Flasar, M., Kunde, V., Lowman, P., Maguire, W., Pearl, J., Pirraglia, J., Samuelson, R., Gautier, D., Gierasch, P., Kumar, S., Ponnamperuma, C., 1979. Infrared observations of the Jovian system from Voyager 1. Science 204, 972–976.

Holweger, H., 2001. Photospheric abundances: problems, updates, implications. In: Wimmer-Schweingruber F. (Ed.), Joint SOHO/ACE Workshop Solar and Galactic Composition. American Institute of Physics Conference Proceedings, 598, 23.

Irwin, P., Weir, A.L, Smith, S.E., Taylor, F.W., Lambert, A.L., Calcutt, S.B., Cameron, P.J., 1998. Cloud structure and atmospheric compostion of Jupiter from Galileo NIMS real-time spectra. J. Geophys. Res. 103 (E10), 23,001–23,022.

Irwin, P.G.J., Weir, A.L., Taylor, F.W., Calcutt, S.B., 2001. The origin of Belt/Zone contrasts in the atmosphere of Jupiter and their correlation with 5-μm opacity. Icarus 149, 397–415.

Kunde, V., Hanel, R., Maguire, W., Gautier, D., Baluteau, J.P., Marten, A., Chedin, A., Husson, N., Scott, N., 1982. The tropospheric gas composition of Jupiter's North Equatorial Belt (NH_3, PH_3, CH_3D, GeH_4, H_2O) and the Jovian D/H ratio. Astrophys. J. 263, 443–467.

Little, B., Anger, C.D., Ingersoll, A.P., Vasavada, A.R., Senske, D.A., Breneman, H.H., Borucki, W.J., 1999. the Galileo SSI Team, Galileo images of lightning on Jupiter. Icarus 142, 306–323.

Niemann, H.B., Atreya, S.K., Garignan, G.R., Donahue, T.M., Haberman, J.A., Harpold, D.N., Hartle, R.E., Hunten, D.M., Kasprzak, W.T., Mahaffy, P.R., Owen, T.C., Way, S.H., 1998. The composition of the Jovian atmosphere as determined by the Galileo probe mass spectrometer. J. Geophys. Res. 103, 22,831–22,846.

Nixon, C.A., Irwin, P.G.J., Calcutt, S.B., Taylor, F.W., 2001. Atmospheric composition and cloud structure in jovian 5-μm hotspots from analysis of Galileo NIMS measurements. Icarus 150, 48–68.

Noll, K., Knacke, R.F., Geballe, T.R., Tokunga, T.A., 1988. The origin and vertical distribution of carbon monoxide in Jupiter. Astrophys. J. 324, 1210–1218.

Noll, K., Larson, H.P., Geballe, T.R., 1990. The abundance of AsH_3 in Jupiter. Icarus 83, 494–499.

Ortiz, J.L., Orton, G.S., Friedson, A.J., Steward, S.T., Fisher, B.M., Spencer, J.R., 1998. The evolution and persistence of 5-μm hot spots at the Galileo probe entry latitude. J. Geophys. Res. 103, 23,051–23,069.

Owen, T., Mahaffy, P.R., Niemann, H.B., Atreya, S.K., Donahue, T., Bar-Nun, A., de Pater, I., 1999. A low-temperature origin for the planetesimals that formed Jupiter. Nature 402, 269–270.

Ragent, B., Colburn, D.S., Avrin, P., Rages, K.A., 1996. Results of the Galileo probe nephelometer experiment. Science 272, 854–856.

Ragent, B., Rages, K.A., Knight, T.C.D., Arvin, P., Orton, G.S., 1998. The clouds of Jupiter: results of the Galileo Jupiter mission probe nephelometer experiment. J. Geophys. Res. 103, 22,891–22,909.

Roos-Serote, M., 1997. Spectro-imagerie infrarouge de Vénus et Jupiter: interprétation des observations Galileo/NIMS. Ph.D. Thesis, University of Paris 6.

Roos-Serote, M., Drossart, P., Encrenaz, T., Lellouch, E., Carlson, R.W, Baines, K.H., Kamp, L., Mehlman, R., 1998. Analysis of Jupiter NEB hot spots in the 4–5 μm range from Galileo/NIMS observations: measurements of cloud opacity, water and ammonia. J. Geophys. Res. 103 (E10), 23,023–23,042.

Roos-Serote, M., Drossart, P., Encrenaz, T., Smith, P.J., Carlson, R.W., 1999. Constraints on the tropospheric cloud structure of Jupiter from spectroscopy in the 5-μm region: a comparison between Voyager/IRIS, Galileo/NIMS and ISO/SWS spectra. Icarus 137, 315–340.

Roos-Serote, M., Vasavada, A.R., Kamp, L., Drossart, P., Irwin, P., Nixon, C., Carlson, R.W., 2000. Proximate humid and dry regions in Jupiter's atmosphere indicate complex local meteorology. Nature 406, 158–160.

Seiff, A., Kirk, D.B., Knight, C.D., Mihalov, J.D., Blanchard, R.C., Young, R.E., Schubert, G., von Zahn, U., Lehman, G., Milos, F.S., Wang, J., 1996. Structure of the atmosphere of Jupiter: Galileo probe measurements. Science 272, 844–845.

Showman, A.P., Dowling, T.E., 2000. Nonlinear simulations of Jupiter's 5-micron hot spots. Science 289, 1737–1740.

Simon-Miller, A.A., Conrath, B., Gierasch, P.J., Beebe, R.F., 2000. A detection of water ice on Jupiter with Voyager IRIS. Icarus 145, 454–461.

Sromovsky, L.A., Best, F.A., Collard, A.D., Fry, P.M., Revercomb, H.E., Freedman, R.S., Orton, G.S., Hayden, J.L., Tomasko, M.G, Lemmon, M.T., 1996. Solar and thermal radiation in Jupiter's atmosphere: initial results of the Galileo Probe Net Flux Radiometer. Science 272, 851–854.

Sromovsky, L.A., Collard, A.D., Fry, P.M., Orton, G.S., Lemmon, M.T., Tomasko, M.G., Freedman, R.S., 1998. Galileo probe measurements of thermal and solar radiation fluxes in the Jovian atmosphere. J. Geophys. Res. 103 (E10), 22,929–22,978.

Weidenschilling, S.J., Lewis, J.S., 1973. Atmospheric and cloud structure of the Jovian planets. Icarus 20, 465–476.